Preprint Title Electronic and Optical Properties of Chloropicrin Adsorbed ZnS Nanotube: First Principle Analysis

Authors Prakash Yadav, Boddepalli SanthiBhushan and Anurag Srivastava

Publication Date 09 Apr. 2025

Article Type Full Research Paper

ORCID® iDs Prakash Yadav - https://orcid.org/0000-0001-9186-8216; Anurag Srivastava - https://orcid.org/0000-0002-7046-405X

Electronic and Optical Properties of Chloropicrin Adsorbed ZnS Nanotube: First Principle Analysis

Prakash Yadav[1], Boddepalli SanthiBhushan[2] and Anurag Srivastava[1*]

[1]Advanced Material Research Group (AMRG), CNT Lab, Department of Engineering Sciences, ABV-Indian Institute of Information Technology and Management, Gwalior, MP-474015, India
[2]Department of Electronics and Communication Engineering, Indian Institute of Information Technology, Allahabad, UP-211015, India
Corresponding email of the author: profanurag@gmail.com

Zinc sulfide nanotubes (ZnS NTs) have garnered significant attention as potential candidates for chemical sensing applications owing to their exceptional structural, electronic, and optical properties. In this study, we employed density functional theory (DFT) to explore the sensing capabilities of a ZnS (3,3) armchair single-walled nanotube (ZnS SWNT) for detecting chloropicrin (CP, CCl_3NO_2), a highly toxic gas. To elucidate the sensing mechanism, we systematically analyze the adsorption configurations, charge transfer, band structure, density of states, optical absorption, and optical conductivity of the ZnS NT-CP system. Our findings reveal that the interaction between CP and ZnS NT induces notable changes in the nanotube's electronic and optical characteristics, including a substantial 40% reduction in the energy band gap for orientation A. Additionally, a good recovery time of 3.5 μs at room temperature, supported by the weak van der Waals-based physisorption phenomenon and significant red shift in the absorption spectra and optical conductivity peaks, highlight ZnS NT's potential for designing reusable CP sensors.

Keywords: Zinc Sulfide nanotube (ZnS NT), Chloropicrin (CP), Chemical sensor.

Introduction

Chloropicrin (CP), also known as trichloronitromethane (CCl_3NO_2), is a chemical warfare agent that poses significant risks of accidental, occupational, and intentional exposure [1], [2]. First synthesized in 1848 by Scottish chemist John Stenhouse via the reaction of picric acid with sodium hypochlorite[3], CP is classified as a Category I toxic agent and is listed as a Schedule II substance under the Chemical Weapons Convention[4]. While its classification permits legal production, storage, and transportation for non-warfare applications, the compound remains a potential hazard due to its dual-use nature.

Recognized as both a choking agent and pulmonary toxicant, CP exhibits potent lachrymatory and ocular irritant properties. Its degradation products, including chlorine, phosgene, nitric oxides, and ammonia, contribute to its toxicity by causing severe pulmonary and ocular damage [5]. Exposure to CP, as depicted in Figure 1, can result in respiratory injuries such as dyspnea, upper respiratory tract damage, and chest pain, even at low concentrations. Severe eye irritation is common, with the corneal epithelium being particularly vulnerable as tear fluid accumulates CP, exacerbating damage. Ocular symptoms can appear within 24 hours of exposure, with studies reporting that 99% of individuals exposed to CP experience ocular symptoms, including inflammation, corneal edema, tissue damage, and potential visual impairment[6], [7], [8].

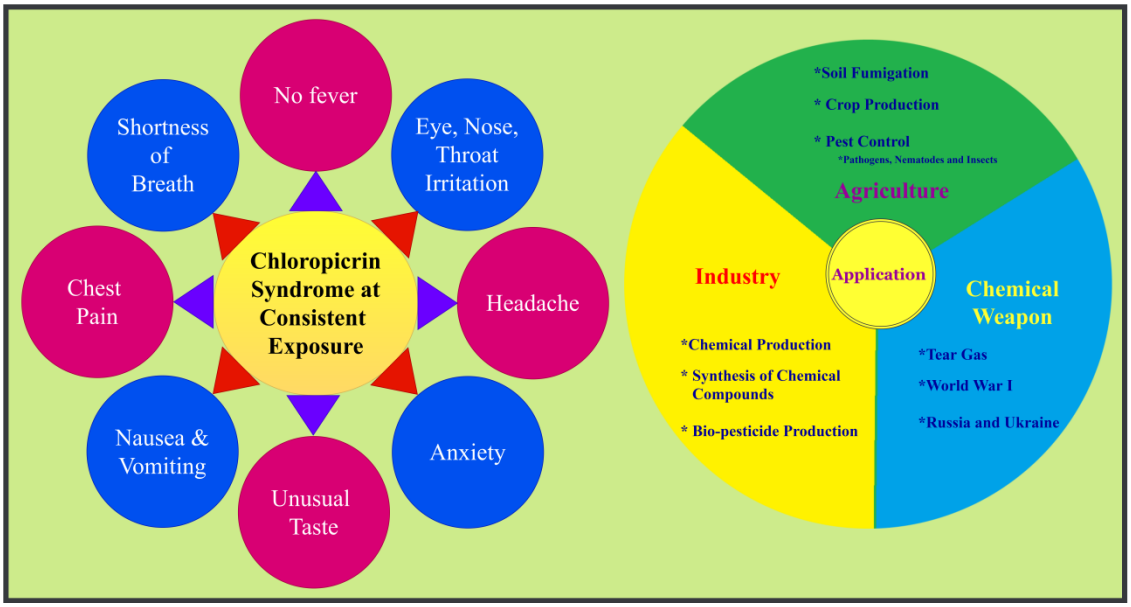

Fig 1. Syndrome at consistent exposure and Applications of Chloropicrin gas

The development of portable, sensitive, rapid-response, and reliable sensors for detecting chemical warfare agents is paramount to ensure safety in agricultural settings and protect public health from potential hazards. Nanomaterials have emerged as an exceptional class of materials, characterized by at least one dimension in the range of 1 to 100 nm. These materials exhibit remarkably high surface areas, which can be tailored through rational design. By precisely controlling their size, shape, synthesis conditions, and functionalization, nanomaterials can achieve extraordinary magnetic, electrical, optical, mechanical, sensing, and catalytic properties that significantly differ from their bulk counterparts [9].

Among the various nanomaterials, zinc sulfide (ZnS) attracts considerable attention due to its unique properties. Nanostructured ZnS has been extensively investigated with different morphologies, including nanotubes, nanowires, nanoparticles, and nanosheets, for applications ranging from ultraviolet light-emitting diodes and injection lasers to flat-panel displays and sensors [10], [11], [12], [13], [14]. ZnS, a promising transition metal chalcogenide with a wide band gap of approximately 3.7 eV, has shown remarkable potential in gas sensing applications. Semiconductor nanomaterials such as graphene, carbon nanotubes, WO_3, ZnO, ZnS, ZnSe, ZnTe, SnO_2, TiO_2, MoS_2, and NiO have been widely employed in gas sensor realization due to their superior selectivity, sensitivity, and response characteristics[15], [16], [17], [18], [19], [20], [21], [22], [23], [24], [25] . ZnS nanotubes are well-suited for gas sensing applications owing to their unique features. These include a high surface area for enhanced gas adsorption, semiconducting properties that enable measurable conductivity changes in the presence of target gases, and their ability to form composites with other materials, such as carbon nanotubes, to optimize performance [21]. Furthermore, the flexible synthesis of ZnS nanotubes with controlled morphology and size allows for tailoring their sensing capabilities. External stimuli like UV light can further enhance their sensitivity and selectivity for specific gases.

These attributes make ZnS nanotubes highly attractive for diverse applications, including detecting volatile organic compounds, choking and pulmonary toxicants, medical diagnostics, and developing portable and wearable gas sensing devices[13], [26], [27], [28], [29], [30], [31], [32], [33], [34].

Previous studies have demonstrated the gas-sensing capabilities of ZnS nanotubes. Md. S. Khan *et al.* [29] investigated ZnS nanotubes as sensors for ammonia and phosphine using density functional theory (DFT) to analyze adsorption behaviour. W. Zhang *et al.* [35] reported that ZnS nanotubes exhibit superior humidity sensing performance compared to ZnO/ZnS nanorod arrays and ZnO nanorod arrays, with enhanced response, faster recovery, good linearity, and reliable reproducibility across a wide range of relative humidity at room temperature. A.K. Giri *et al.* [36] demonstrated that phase-selective ZnO@ZnS heterostructures and ZnS nanotubes exhibited superior amperometric cholesterol sensing performance, with ZnS nanotubes achieving the highest sensitivity (598 mA/m^2) and low detection limits among the configurations studied.

Despite these advances, the use of ZnS nanotubes for detecting chloropicrin (CP), a highly toxic chemical warfare agent, remains an area with untapped potential. Addressing this gap, the present work constructs an armchair ZnS nanotube to investigate its adsorption configurations, charge transfer, band structure, density of states, optical absorption, and optical conductivity using a density functional theory-based approach. Our findings suggest that ZnS nanotubes are promising candidates for the development of advanced sensors for detecting chemical warfare agents, with potential applications in safety, environmental monitoring, and public health protection.

Computational Methodology

The computational analyses were conducted using linear combination of atomic orbitals (LCAO) density functional theory (DFT) approach, as implemented in the Synopsys-QuantumATK software. Electron exchange-correlation interaction energies were calculated using the Generalized Gradient Approximation (GGA) with the Revised Perdew-Burke-Ernzerhof (RPBE) parameterization. Pseudo-atomic double zeta double polarized (DZDP) basis sets were utilized to define the atomic orbitals. Brillouin zone sampling was performed using a Monkhorst-Pack grid of k-points set to 1*1*100, ensuring accurate representation of periodic boundary conditions along the nanotube's axis. A density mesh cutoff of 150 Rydberg was applied to define the real-space grid for energy calculations.

The ZnS nanotube model, consisting of 36 atoms arranged periodically along the Z-direction, was structurally optimized to achieve geometric and energetic stability. Optimization was performed with stringent convergence criteria: a maximum force tolerance of 0.05 eV/Å and a stress tolerance of 0.05 $eV/Å^3$. These parameters ensured the reliability and accuracy of the resulting structural configurations for subsequent electronic and transport property analyses.

To study the optical properties of the ZnS Nanotube without and with molecular adsorption, we calculated the absorption coefficient (α), and optical conductivity σ , which can be obtained by the following formula[16]:

$$\alpha = \sqrt{2}\frac{\omega}{c}\left(\sqrt{\varepsilon_1^2 + \varepsilon_2^2} - \varepsilon_1\right)^{\frac{1}{2}} \qquad -(01)$$

$$\sigma = \frac{n\alpha c}{4\pi} \qquad -(02)$$

Where ω is the angular frequency of light, ε_1 and ε_2 are real and imaginary part of the complex permittivity, n is the refractive index of materials, and c is the speed of light. The real part of the optical conductivity is related to the absorption of light, while the imaginary part is related to the dispersion.

Results and Discussion

Structural Analysis

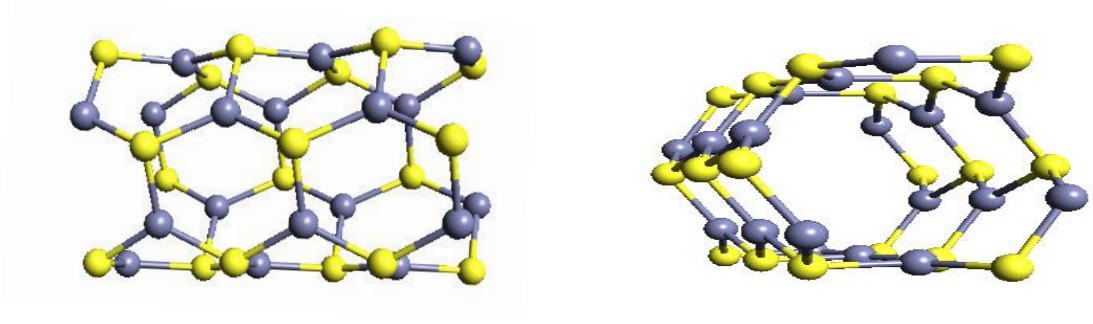

(a) **(b)**

Fig 2. Optimized pristine ZnS NT (a) Side View (b) Front View

The optimized geometry of the armchair ZnS nanotube with (3,3) chirality is illustrated in Fig.2. The structural analysis reveals an average Zn–S bond length of 2.29 Å, which is slightly shorter than the bond length of bulk ZnS (2.34 Å). This reduction in bond length can be attributed to the curvature of the nanotube structure, which induces slight strain in the lattice. A vacuum slab of 20 Å thickness was introduced along the radial direction to minimise spurious interactions between adjacent nanotube images in the simulation. This ensures that the periodic boundary conditions do not artificially influence the electronic and structural properties of the nanotube.

The cohesive energy (E_C) $per\ atom\ of\ ZnS\ NT$ is calculated using the Equation.(3) [37].

$$E_C = \frac{1}{a+b}[E_{ZnS\,NT} - aE_{Zn} - bE_S] \qquad -(03)$$

Where, $E_{ZnS\,NT}$, E_{Zn} and E_S illustrate the corresponding energy of pristine ZnS NT, isolated Zn and S atoms, respectively. The number of Zn and S atoms in pristine ZnS NT are referred to as 'a' and 'b', respectively.

Table 1 shows the Cohesive energy (EC), which is the energy required to break the nanotube into individual atoms, the average diameter between two opposite sulfurs (d_S) and Zincs (d_{Zn}), and the radial buckling δ.

Table 1: The cohesive energy (E_C), average diameter between two opposite sulfurs (d_S) and Zincs (d_{Zn}), and the radial buckling δ of the armchair ZnS NT.

Nanotube	**Cohesive Energy E_C (eV/atom)**	**d_S (nm)**	**d_{Zn} (nm)**	**δ (nm)**
ZnS NT(3,3)	-3.832	0.708	0.618	0.09

The cohesive energy of the ZnS nanotube (ZnS NT) is calculated to be -3.832 eV/atom. This negative formation energy indicates that the formation of ZnS NT from its constituent elements is energetically favorable, signifying an exothermic process. In such reactions, the energy required to break the bonds in the reactants is less than the energy released during the formation of new bonds in the product, confirming the thermodynamic stability of the nanotube structure. Although these single-walled nanotubes (SWNTs) are derived from flat hexagonal ZnS sheets, the resulting structures exhibit slight deviations from perfect smoothness. Specifically, a small radial anion-cation buckling of approximately ±0.1 Å was observed, consistent with previous reports on reconstructed ZnS SWNTs [[38][27], [38], [39], [40]]. This minor buckling is attributed to the inherent curvature induced during the transition from a planar sheet to a tubular form.

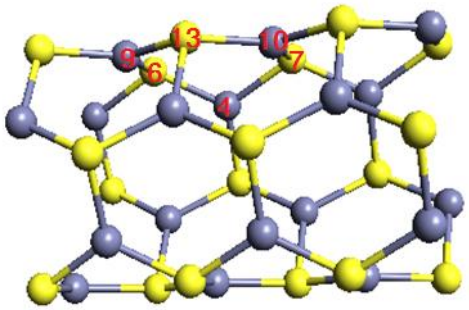

(i)

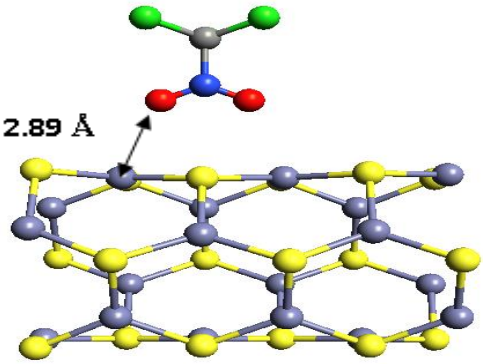

(ii) Orientation-A

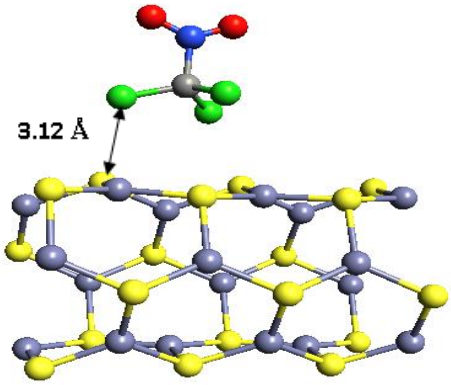

(iii) Orientation-B

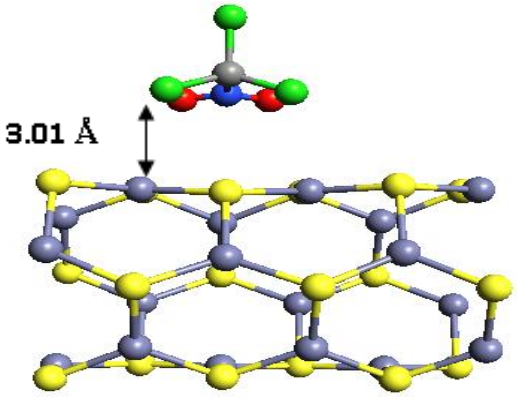

(iv) Orientation-C

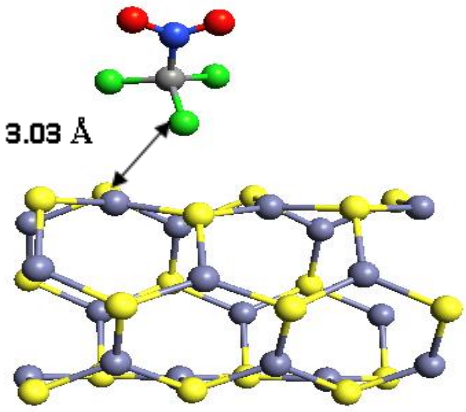

(v) Orientation-D

Fig 3. Favourable molecular orientation for the adsorption of CP molecule on ZnS NT structure.

The presence of buckling in the nanotube structure is of significant interest due to its potential implications for surface properties. The buckling could form a surface dipole, enhancing the nanotube's interaction with external molecules. Such structural features are particularly

relevant for potential applications in gas sensing, where surface interactions play a critical role in sensitivity and selectivity.

The adsorption energies for Chloropicrin(CP) with different adsorption orientations on pristine ZnS NT have been calculated using the equation (04) [29].

$$E_{Ads} = E_{(CP\ adsorbed\ ZnS\ NT)} - (E_{ZnS\ NT} + E_{CP}) \qquad -(04)$$

where $E_{CP\ adsorbed\ ZnS\ NT)}$, $E_{ZnS\ NT}$ and E_{CP} corresponds to the energies of CP adsorbed ZnS nanotube, isolated ZnS nanotube and isolated CP, respectively.

The adsorption behavior of CP on the ZnS nanotube surface was analyzed for four distinct molecular orientations, denoted as A, B, C, and D, in Fig.3. adsorption energies for these orientations are calculated and presented in Table 4, with values of -0.389 eV, -0.657 eV, -0.593 eV, and -0.440 eV for A, B, C and D orientations driven by the physisorption phenomenon, respectively. Among the four orientations, B is identified as the most favourable one with the lowest adsorption energy due to the interaction between the chlorine atoms of CP and the Zn site of ZnS NT. It is to be noted from the different orientations that the chlorine atoms of CP tend to interact strongly with the ZnS NT surface in comparison to the oxygen atoms of CP, which may be attributed to the availability of 3 lone pairs with each chlorine atom in comparison to the 2 lone pairs with each oxygen atoms. To gain deeper insight into the nature of these interactions, Mulliken population analysis was performed, revealing the extent of electronic charge transfer from CP to ZnS NT for each orientation of molecule (see Table.4). The corresponding charge transfers are 0.073e, 0.095e, 0.109e, and 0.06e for orientations A, B, C, and D, respectively.

The electronic charge transfer led by the weak physisorption phenomenon plays a critical role in altering the electronic and optical properties of ZnS NT. A higher charge transfer improves sensor sensitivity, allowing the detection of CP at lower concentrations, whereas the weak physisorption led by the van der Waals forces may help with the reusability of sensor devices.

Table 2: Variations in the Zn-S bond length of ZnS NT near the CP adsorption site.

S.No.	The Bond length between the Zn-S atomic position	Pristine ZnS NT	Orientation A		Orientation B		Orientation C		Orientation D	
		bond length (in Å) before optimization	bond length (in Å)	Change bond-length dl (in Å)	bond length (in Å)	Change bond-length dl (in Å)	bond length (in Å)	Change bond-length dl (in Å)	bond length (in Å)	Change bond-length dl (in Å)
			after optimization		after optimization		after optimization		after optimization	
1	Zn-S (13-9)	2.324	2.319	0.005	2.309	0.015	2.312	0.012	2.310	0.014
2	Zn-S (9-6)	2.267	2.273	-0.006	2.270	-0.003	2.256	0.011	2.266	0.001
3	Zn-S (6-4)	2.316	2.319	-0.003	2.305	0.011	2.305	0.011	2.316	0
4	Zn-S (4-7)	2.317	2.319	-0.002	2.313	0.004	2.309	0.008	2.324	-0.007
5	Zn-S (7-10)	2.265	2.281	-0.016	2.263	0.002	2.256	0.009	2.266	-0.001
6	Zn-S (10-13)	2.321	2.316	0.005	2.302	0.019	2.309	0.012	2.295	0.026
7	Adsorption distance of CP molecule		2.89 **Å**		3.01 **Å**		3.12 **Å**		3.03 **Å**	

Table 2 highlights the changes in Zn-S bond lengths near the CP adsorption site for different orientations before and after optimization, alongside the adsorption distance between the adsorbate and adsorbent. The most significant changes in bond length were observed near the atomic positions Zn(10)-S(13)-Zn(9), which correspond to the maximum structural deformation caused by CP physisorption. These results are consistent with the adsorption energy trends.

Band Structures and Density of States Analysis

The electronic properties of ZnS nanotubes (ZnS NTs) in the presence of CP molecules are analyzed with the help of band structure, total as well as partial densities of states (DOS)

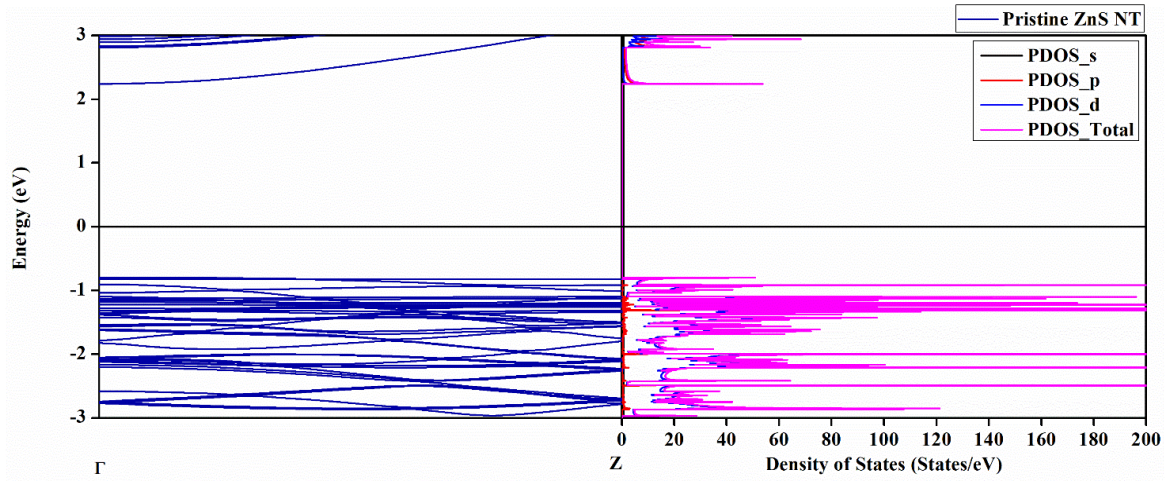
Pristine ZnS NT
PDOS_s
PDOS_p
PDOS_d
PDOS_Total
Energy (eV)
3
2
1
0
-1
-2
-3
Γ
Z
0 20 40 60 80 100 120 140 160 180 200
Density of States (States/eV)

(i)

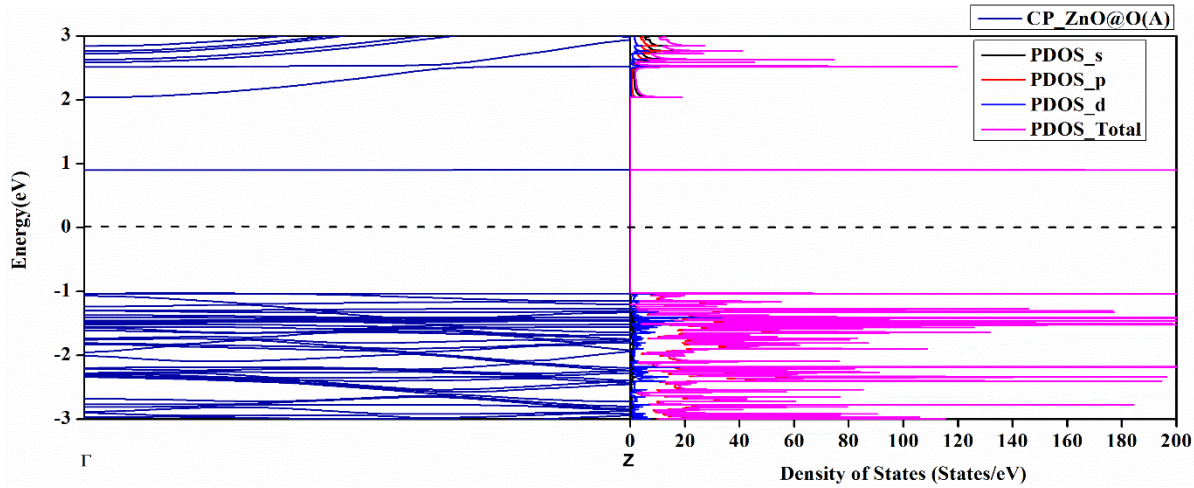
CP_ZnO@O(A)
PDOS_s
PDOS_p
PDOS_d
PDOS_Total
Energy(eV)
3
2
1
0
-1
-2
-3
Γ
Z
0 20 40 60 80 100 120 140 160 180 200
Density of States (States/eV)

(ii)

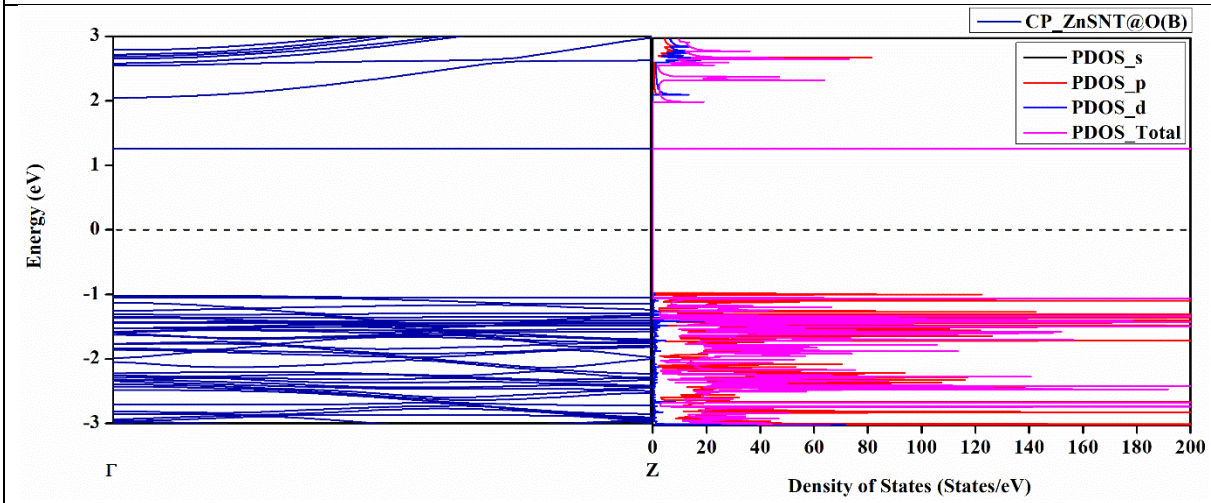
CP_ZnSNT@O(B)
PDOS_s
PDOS_p
PDOS_d
PDOS_Total
Energy (eV)
3
2
1
0
-1
-2
-3
Γ
Z
0 20 40 60 80 100 120 140 160 180 200
Density of States (States/eV)

(iii)

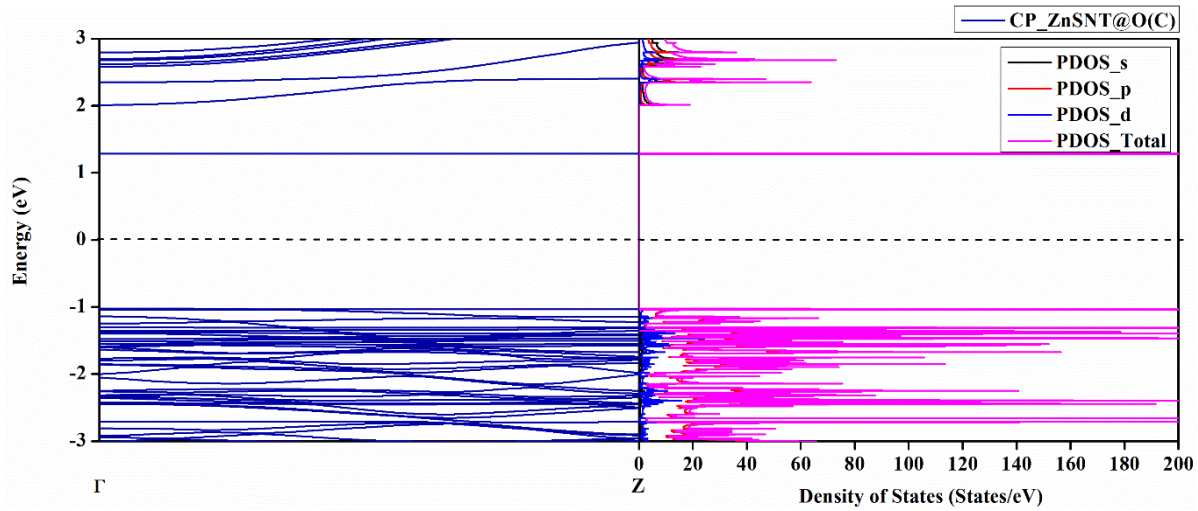

(iv)

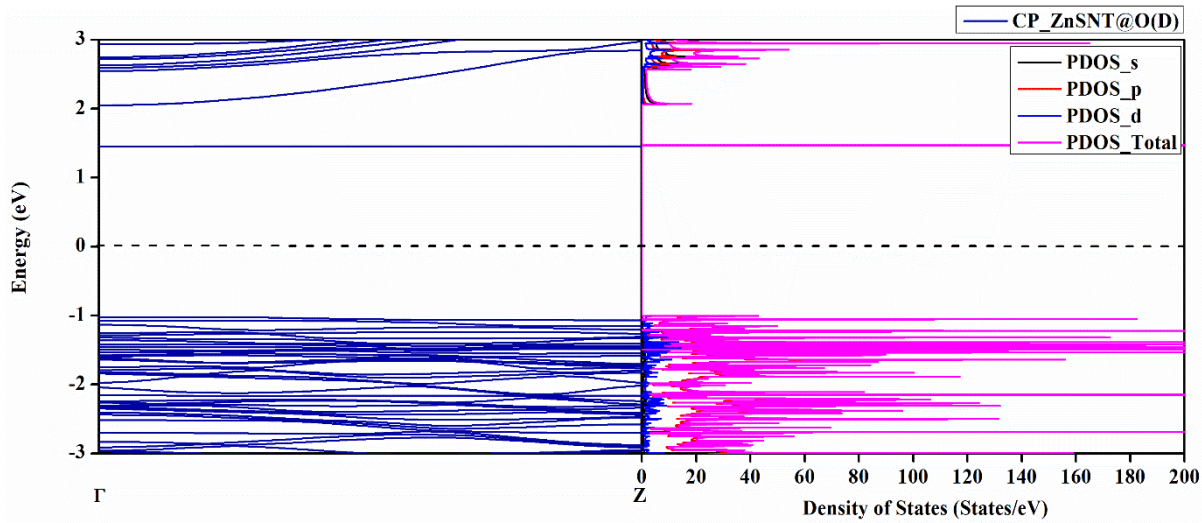

(v)

Fig 4. Band structure and PDOS profiles of (i) Pristine ZnS nanotube, (ii) **A,** (iii) **B**, (iv) **C** and (v) **D** orientations of CP adsorbed ZnS nanotube.

calculations. This analysis provides critical insights into how the adsorption of CP molecule affects the electronic behavior of the nanotube.

The band structure and DOS profile for pristine ZnS NT and CP-adsorbed ZnS NT in orientations A, B, C, and D are shown in Fig.4. The pristine ZnS NT exhibits a band gap of 3.03 eV (Figure 3(i)), consistent with previous studies [27], [29], [38], [39], [40], [41], [42]. Upon CP adsorption, the band gap values for orientations A, B, C, and D were reduced to 1.92 eV, 2.27 eV, 2.31 eV, and 2.47 eV, respectively. This reduction in the band gap is evident from the band spectra and highlights the electronic interaction between CP and ZnS NT. The most prominent reduction of 58% is observed for orientation A. The decrease in the band gap infers improved electronic conductivity of ZnS NT upon exposure to CP.

The DOS profiles show additional peaks in the ZnS NT system upon CP adsorption. Notably, the interaction of CP introduces distinct states near both the conduction and valence bands. Unlike the pristine ZnS NT, the DOS of CP adsorbed ZnS NTs show new peaks around 1 eV (relative to the Fermi level) energy of the conduction band. These peaks have the contributions of the 2p orbitals of CP molecule and the d orbitals of Zn. For all CP orientations, the filled valence bands near -1 eV (relative to the Fermi level) energy primarily consist of states from the d orbitals of Zn and the p orbitals of S.

Based on Koopman's theorem [[43], [44]], the highest-occupied molecular orbital energy (EHOMO) of the target molecule has been employed to estimate the ionization potential (IP), while the lowest-unoccupied molecular orbital energy (ELUMO) correlates with electron affinity (EA). According to Mulliken's definition [[44]], the average of these two energies yields electronegativity (χ), expressed as shown in Equation (05).

$$\chi = \frac{(EA + IP)}{2} \qquad -(05)$$

Table 3: Ionization energy, electronegativity and electron affinity of target CP molecules for orientations A, B, C and D on the ZnS NT Surface.

Target Molecule Orientation	Ionization energy (eV)	Electron Affinity (eV)	Electronegativity (eV)
CP_ZnSNT@O (A)	0.611	0.905	0.758
CP_ZnSNT@O (B)	0.710	1.453	1.081
CP_ZnSNT@O (C)	0.717	1.288	1.003
CP_ZnSNT@O (D)	0.704	1.260	0.982

Ionization potential is defined as the energy required to remove an electron from the molecule, whereas electron affinity refers to the energy released when an electron is added to the molecule. The calculated IP and EA values for the target molecules are summarized in Table 3. Ionization potential is critical for assessing chemical reactivity; high IP values indicate chemical inertness and greater stability, whereas low IP values suggest higher molecular reactivity. The results show that the lower IP values of the target molecules make them more likely to donate electrons to the acceptor system.

Table 4: The adsorption energy E_{Ads}, Bandgap E_g, % change in bandgap $\Delta E_g(sensitivity)$, charge transfer, and recovery time of the armchair ZnS NTs at orientation A, B, C, and D, respectively.

S.No	Orientation of Molecule	Adsorption Energy E_{Ads} (eV)	Bandgap E_g (eV)	% Change in Bandgap, ΔE_g	Charge Transfer Q (e)	Recovery Time τ (s)
01	Pristine ZnS NT	-	3.17	-	-	-
02	CCl_3NO_2 - ZnS NT (A)	-0.389	1.92	40	0.073	3.533 µs
03	CCl_3NO_2- ZnS NT (B)	-0.657	2.27	29.6	0.095	0.114 s
04	CCl_3NO_2- ZnS NT (C)	-0.593	2.31	27	0.109	9.60 ms
05	CCl_3NO_2- ZnS NT (D)	-0.440	2.47	23	0.06	25.50 µs

The percentage change in energy band gap for CP adsorption on ZnS NT (see Table 4) are noted as 40%, 29.6%, 27%, and 23% for orientations A, B, C, and D, respectively. Among these, the most significant variation in the energy gap is observed for orientation A. Consequently, the conductivity of ZnS NT exhibits a significant variation, demonstrating its suitability for sensing applications.

The sensitivity of the sensor is defined in terms of the change in the band gap[45] by using the following equation 06

$$\Delta E_g = \frac{(E_{g2} - E_{g1})}{E_{g1}} * 100 \qquad -(06)$$

Where E_{g1} and E_{g2} are the band gap of the pristine ZnS NT and CP adsorbed ZnS NT, respectively.

Recovery time[5], [35], [46] is influenced by the adsorption energy, as described by the conventional transition state theory

$$\tau = \vartheta_0^{-1} e^{\left(\frac{-\Delta E_{ads}}{K_B T}\right)} \qquad -(08)$$

Where T is the Temperature (= 300^0C), K_B Is the Boltzmann's constant ($8.617x10^{-5}$ eV/K), and ϑ_0 is the attempt frequencies (=10^{12} Hz).

The recovery time of ZnS NT for various orientations of CP adsorption are calculated and presented in Table.4.

Table 5: Comparison of sensing response, and recovery time with previous works.

Materials	Target molecules	Sensing Response	Recovery time	References
Kagome Phosphorene	Chloropicrin, Phosgene	58.28%	-	[12]
BN nanocones	Chloropicrin	84.1%	37 μs at 298K	[47]
pristine nanographenes	Chloropicrin	41.1%	-	[48]
borazine-doped nanographenes	Chloropicrin	39.7%	14.6 s at 350K	[48]
Silicon Carbide CP@C_$Si_{12}C_{12}$ Nanocluster	Chloropicrin	28.8%	5.98×10^{29} s	[37]
CP@Si_$Si_{12}C_{12}$ Nanocluster	Chloropicrin	35.4%	4.38×10^{29} s	[37]
Green Phosphorene Nanotube	Adamsite and Chloropicrin	41.4%	-	[49]
ZnS Nanotube	*Chloropicrin*	*40%*	*3.5 μs* at 300 K	*Present Work*

Remarkably, the sensing response and recovery time of ZnS NT towards CP molecule for orientation A is found to be particularly favorable. Notably, the recovery time of ZnS NT for orientation A is estimated as 3.5 μs at 300 K, the fastest among all previous works related to CP adsorption listed in Table.5, underscoring its exceptional potential for real-time sensing applications.

Optical Properties

The absorption spectra of pristine ZnS nanotubes (NTs) and CP-adsorbed ZnS NTs at orientations A, B, C, and D reveal significant variations that elucidate the interaction mechanisms between CP molecules and ZnS NTs. For pristine ZnS NTs, the spectrum displays multiple sharp peaks in the UV region (250–400 nm), with the strongest peak occurring at approximately 290–300 nm. This behavior is attributed to the intrinsic wide bandgap of ZnS (~3.68 eV), which confines its absorption to the UV range, as confirmed by both experimental and theoretical studies on ZnS nanostructures[50]. These peaks arise from interband electronic transitions between the valence and conduction bands, reflecting the material's fundamental optical properties. Furthermore, the absence of significant absorption in the visible region (>400 nm) underscores the lack of mid-gap states in pristine ZnS NTs. Such optical characteristics align with previous reports highlighting ZnS nanostructures' suitability for UV

photodetectors, sensors and photocatalytic applications, where high UV sensitivity is critical[51].

Upon CP molecule adsorption, significant redshifts in the absorption spectra are observed across all orientations, indicative of bandgap narrowing caused by molecular interactions. Among the orientations, Orientation A shows the most pronounced effect, with a strong absorption peak appearing in the visible range (500–600 nm). This redshift is directly linked to the formation of mid-gap electronic states induced by charge transfer from the CP molecule to the ZnS NT. Such changes in the electronic structure are consistent with density functional theory (DFT) studies that demonstrate adsorption-induced bandgap modulation in semiconducting nanostructures. The enhanced absorption intensity observed in Orientation A reflects strong coupling between the adsorbed CP molecule and the ZnS NT, highlighting this configuration as the most effective for modulating optical properties. This pronounced shift into the visible range makes Orientation A particularly suitable for optical sensing applications, where small molecular interactions can induce detectable spectral changes [52].

In contrast, Orientation B exhibits a reduced absorption intensity in the UV range, with a weaker secondary peak in the visible range (400–500 nm). This suggests a weaker interaction between the CP molecule and the ZnS NT, likely due to less favourable adsorption geometry. Consequently, the bandgap modification is less pronounced compared to Orientation A, resulting in moderate optical tuning. Such orientation-dependent optical responses are consistent with prior studies on ZnS NTs, where adsorption sites and molecular orientation strongly influence electronic coupling and optical transitions [53]. Orientation C displays a broader absorption spectrum with multiple peaks spanning both the UV (250–400 nm) and visible (400–700 nm) regions. The visible range peaks, though less intense than in Orientation A, are broader, indicating complex interactions between the CP molecule and the ZnS NT. This could arise from the adsorption of CP molecules at multiple active sites or a combination of adsorption geometries, as previously observed in DFT-based studies on nanostructure-molecule interactions [54]. The presence of multiple optical transitions suggests moderate bandgap narrowing and indicates potential for broader spectral sensitivity, making Orientation C a versatile configuration for applications requiring multi-wavelength optical detection. Orientation D, on the other hand, shows absorption spectra similar to that of pristine ZnS NT, with only a slight redshift and weak absorption in the visible range. This suggests that the interaction between CP molecules and ZnS NT in Orientation D is minimal, resulting in negligible modifications to the electronic structure. Such weak adsorption effects are consistent with configurations where molecular interactions are dominated by van der Waals forces rather than strong charge transfer or dipole interactions [55].

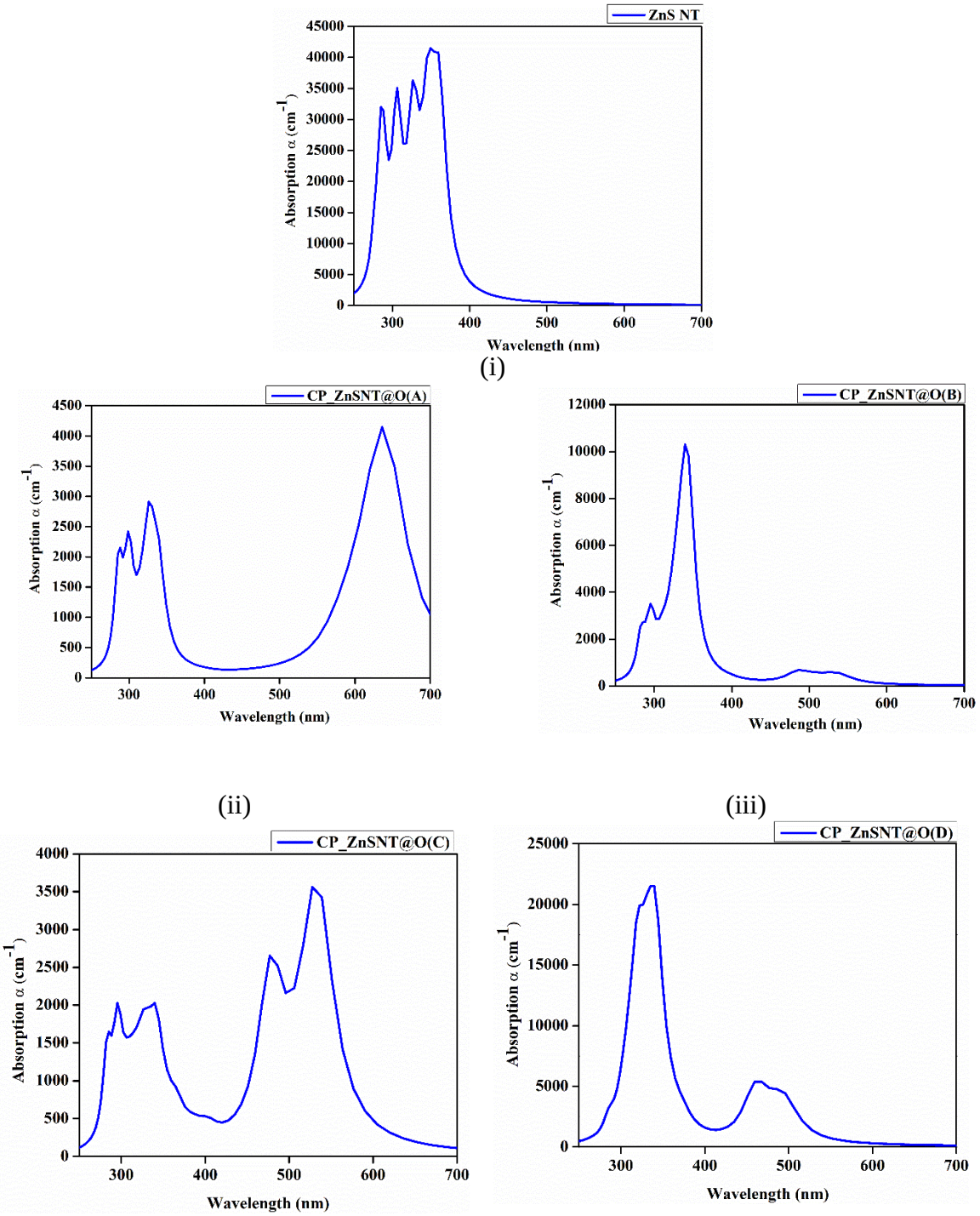

Fig 5. Absorption Spectra (in YY-direction) for (i) Pristine ZnS nanotube, (ii) **A,** (iii) **B**, (iv) **C** and (v) **D** orientations of CP adsorption on ZnS nanotube

The anisotropic nature of ZnS NTs plays a significant role in the observed orientation-dependent optical responses. Adsorption along orientations such as A induces stronger dipole interactions and greater charge transfer, leading to more pronounced bandgap narrowing and enhanced visible light absorption. This anisotropic behaviour is consistent with theoretical and experimental studies on nanotubular systems, where adsorption-induced optical changes are highly dependent on molecular orientation and the local electronic environment [56]. The

redshifts observed in the visible range for CP-adsorbed ZnS NTs highlight the tunability of their optical properties, particularly in Orientation A, which exhibits the strongest response. Such behaviour demonstrates the suitability of ZnS NTs as optical sensors capable of detecting CP molecules with high sensitivity and specificity.

The optical conductivity spectra of pristine ZnS NTs and CP-adsorbed ZnS NTs at orientations A, B, C, and D reveal significant orientation-dependent variations due to CP adsorption. Pristine ZnS NTs exhibit a dominant peak in the real part ($\sigma_1(\omega)$) at ~395 nm, consistent with interband transitions of ZnS (~3.68 eV), and a peak in the imaginary part ($\sigma_2(\omega)$) at ~290 nm, representing stored energy. These UV absorption properties align with the wide bandgap of ZnS, making it suitable for UV photodetectors and photocatalysis.

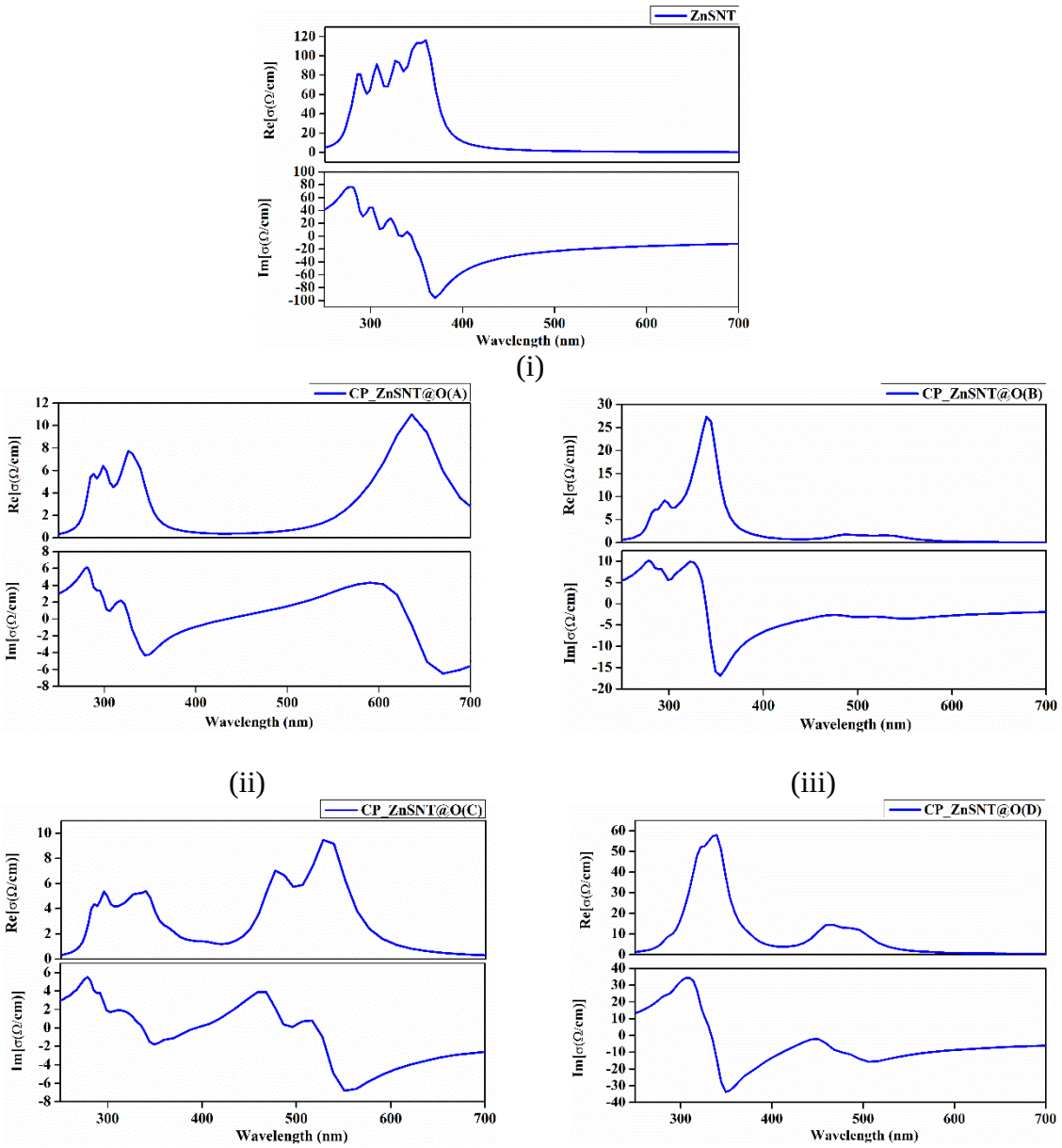

Fig 6. Optical Conductivity (in YY-direction) for (i) Pristine ZnS nanotube, (ii) **A,** (iii) **B**, (iv) **C** and (v) **D** orientations of CP adsorption on ZnS nanotube

CP adsorption induces redshifts in $\sigma_1(\omega)$ and $\sigma_2(\omega)$, reflecting bandgap narrowing. Orientation A shows the most significant redshift ($\sigma_1(\omega)$) peak at ~630 nm, attributed to mid-gap state formation due to strong charge transfer, enhancing visible light absorption for sensing applications. Orientation B exhibits a smaller redshift (~410 nm), indicating weaker interaction. Orientation C shows multiple peaks across UV and visible ranges, suggesting complex adsorption behaviour. Orientation D exhibits negligible shifts, dominated by van der Waals forces.

These findings demonstrate the anisotropic optical behaviour of ZnS NTs, with Orientation A offering the strongest potential for optical sensing, while others show moderate or limited tuning, supporting tailored optoelectronic applications.

Conclusion

In conclusion, this work uses first-principles simulations to discuss the adsorption of Chloropicrin (CP) on ZnS nanotubes (ZnS NTs). The adsorption configurations, charge transfer, band structure, density of states, optical absorption, and optical conductivity have been systematically analysed. The adsorption of CP induces substantial modifications in the nanotube's optical and electronic properties, including a remarkable 40% reduction in the energy band gap, a high recovery time of 3.5 μs at room temperature supported by the weak van der Waals-based physisorption phenomenon and significant red shift in the absorption coefficient and optical conductivity peaks. The results underscore the potential of ZnS NT as a sensor material for CP and the suitability for realizing reusable sensors.

Acknowledgement

The authors express their gratitude to the Atal Bihari Vajpayee - Indian Institute of Information Technology and Management (ABV-IIITM) Gwalior for providing the infrastructural support during this research. PY extends gratitude to the Ministry of Education, Government of India, for the doctoral fellowship.

AI Tools Usage

ChatGPT was used only to improve the manuscript's English.

Ethical Approval

'Not Applicable'

Consent to Participate

'Not Applicable'

Consent to Publish

'Not Applicable'

Authors Contributions

P.Y.: Conceptualization, DFT Calculation, Result analysis and Manuscript writing

B.S.: Scientific discussion, Review and Editing

A. S.: Conceptualization, Supervision, Review and Editing

Funding

The authors declare that no funds, grants, or other support were received during the preparation of this manuscript.

Competing Interests

The authors have no relevant financial or non-financial interests to disclose.

References

[1] M. Pesonen and K. Vähäkangas, "Chloropicrin-induced toxicity in the respiratory system," *Toxicol. Lett.*, vol. 323, no. January, pp. 10–18, 2020, doi: 10.1016/j.toxlet.2020.01.022.

[2] Y. Zhou, Z. X. Ye, H. Huang, Y. D. Liu, and R. Zhong, "Formation mechanism of chloropicrin from amines and free amino acids during chlorination: A combined computational and experimental study," *J. Hazard. Mater.*, vol. 416, no. April, p. 125819, 2021, doi: 10.1016/j.jhazmat.2021.125819.

[3] S. E. Sparks, G. B. Quistad, and J. E. Casida, "Chloropicrin: Reactions with biological thiols and metabolism in mice," *Chem. Res. Toxicol.*, vol. 10, no. 9, pp. 1001–1007, 1997, doi: 10.1021/tx9700477.

[4] S. Mukherjee *et al.*, *Vesicants and Oxidative Stress*, no. August 2019. 2007. doi: 10.1201/9781420046625.ch12.

[5] B. Muir, W. A. Carrick, and D. B. Cooper, "Application of central composite design in the optimisation of thermal desorption parameters for the trace level determination of the chemical warfare agent chloropicrin," *Analyst*, vol. 127, no. 9, pp. 1198–1202, 2002, doi: 10.1039/b204782a.

[6] S. Gaskin, L. Heath, D. Pisaniello, J. W. Edwards, M. Logan, and C. Baxter, "Dermal absorption of fumigant gases during HAZMAT incident exposure scenarios - Methyl bromide, sulfuryl fluoride, and chloropicrin," *Toxicol. Ind. Health*, vol. 33, no. 7, pp. 547–554, 2017, doi: 10.1177/0748233716689651.

[7] L. R. Goldman, D. Mengle, D. M. Epstein, D. Fredson, K. Kelly, and R. J. Jackson, "Acute symptoms in persons residing near a field treated with the soil fumigants methyl bromide and chloropicrin," *West. J. Med.*, vol. 147, no. 1, pp. 95–98, 1987.

[8] A. Kumar *et al.*, "Highly responsive and low-cost ultraviolet sensor based on ZnS/p-Si heterojunction grown by chemical bath deposition," *Sensors Actuators, A Phys.*, vol. 331, p. 112988, 2021, doi: 10.1016/j.sna.2021.112988.

[9] L. Y. Zhu, L. X. Ou, L. W. Mao, X. Y. Wu, Y. P. Liu, and H. L. Lu, *Advances in Noble Metal-Decorated Metal Oxide Nanomaterials for Chemiresistive Gas Sensors: Overview*, vol. 15, no. 1. Springer Nature Singapore, 2023. doi: 10.1007/s40820-023-01047-z.

[10] X. Fang *et al.*, "ZnS nanostructures: From synthesis to applications," *Prog. Mater. Sci.*, vol. 56, no. 2, pp. 175–287, 2011, doi: 10.1016/j.pmatsci.2010.10.001.

[11] W. Feng *et al.*, "Atomically thin ZnS nanosheets: Facile synthesis and superior piezocatalytic H2 production from pure H2O," *Appl. Catal. B Environ.*, vol. 277, no. June 2020, p. 119250, 2020, doi: 10.1016/j.apcatb.2020.119250.

[12] J. Princy Maria, R. Bhuvaneswari, V. Nagarajan, and R. Chandiramouli, "Kagome phosphorene molecular device for sensing chloropicrin and phosgene – A first-principles study," *Chem. Phys. Lett.*, vol. 771, no. February, p. 138472, 2021, doi: 10.1016/j.cplett.2021.138472.

[13] Y. S. Tsai, X. D. Lin, Y. S. Wu, H. Chen, and J. Han, "Dual UV Light and CO Gas Sensing Properties of ZnO/ZnS Hybrid Nanocomposite," *IEEE Sens. J.*, vol. 21, no. 9, pp. 11040–11045, 2021, doi: 10.1109/JSEN.2021.3057617.

[14] Jogender, B. Badhani, Mandeep, and R. Kakkar, "A DFT-D2 study on the adsorption of phosgene derivatives and chloromethyl chloroformate on pristine and Fe4-decorated graphene," *J. Mol. Graph. Model.*, vol. 101, p. 107754, 2020, doi: 10.1016/j.jmgm.2020.107754.

[15] M. K. Hazrati, Z. Bagheri, and A. Bodaghi, "Application of C 30 B 15 N 15 heterofullerene in the isoniazid drug delivery: DFT studies," *Phys. E-low-dimensional Syst. Nanostructures*, vol. 89, pp. 72–76, 2017, doi: 10.1016/J.PHYSE.2017.02.009.

[16] X. Cai, S. Deng, L. Li, and L. Hao, "A first-principles theoretical study of the electronic and optical properties of twisted bilayer GaN structures," *J. Comput. Electron.*, vol. 19, no. 3, pp. 910–916, 2020, doi: 10.1007/s10825-020-01512-7.

[17] K. A. Soliman and S. A. Aal, "Ti, Ni, and Cu decorated borospherene as potential molecular sensor for phosgene," *Mater. Sci. Semicond. Process.*, vol. 144, no. October 2021, p. 106574, 2022, doi: 10.1016/j.mssp.2022.106574.

[18] M. S. Khan, A. Sharma, M. S. Khan, A. Srivastava, and M. Husain, "Si-doped MoS2 sheet as phosgene gas sensor: A first principles study," *AIP Conf. Proc.*, vol. 2115, no. July, pp. 1–5, 2019, doi: 10.1063/1.5113277.

[19] M. Noei, "Different electronic sensitivity of BN and AlN nanoclusters to SO2 gas: DFT studies," *Vacuum*, vol. 135, pp. 44–49, 2017, doi: 10.1016/J.VACUUM.2016.10.029.

[20] L. Saedi, S. Jameh-bozorghi, M. Maskanati, and H. Soleymanabadi, "The effect of water on the electronic and field emission properties of inorganic AlN nanocones: Computational study," *Inorg. Chem. Commun.*, vol. 90, pp. 86–91, 2018, doi: 10.1016/J.INOCHE.2018.02.011.

[21] H. Soleymanabadi and J. Kakemam, "A DFT study of H2 adsorption on functionalized carbon nanotubes," *Phys. E-low-dimensional Syst. Nanostructures*, vol. 54, pp. 115–117, 2013, doi: 10.1016/J.PHYSE.2013.06.015.

[22] S. F. Rastegar, N. Hadipour, M. B. Tabar, and H. Soleymanabadi, "DFT studies of acrolein molecule adsorption on pristine and Al- doped graphenes," *J. Mol. Model.*, vol. 19, pp. 3733–3740, 2013, doi: 10.1007/s00894-013-1898-5.

[23] S. Jameh-bozorghi and H. Soleymanabadi, "Warped C 80 H 30 nanographene as a chemical sensor for CO gas: DFT studies," *Phys. Lett. A*, vol. 381, pp. 646–651, 2017, doi: 10.1016/J.PHYSLETA.2016.11.039.

[24] Z. Rostami, M. Pashangpour, and R. Moradi, "DFT study on the chemical sensing properties of B24N24 nanocage toward formaldehyde.," *J. Mol. Graph. Model.*, vol. 72, pp. 129–135, 2017, doi: 10.1016/j.jmgm.2016.12.013.

[25] M. Nayebzadeh, A. A. Peyghan, and H. Soleymanabadi, "Density functional study on the adsorption and dissociation of nitroamine over the nanosized tube of MgO," *Phys. E-low-dimensional Syst. Nanostructures*, vol. 62, pp. 48–54, 2014, doi: 10.1016/J.PHYSE.2014.04.016.

[26] P. D'Amico, A. Calzolari, A. Ruini, and A. Catellani, "New energy with ZnS: Novel applications for a standard transparent compound," *Sci. Rep.*, vol. 7, no. 1, pp. 1–9, 2017, doi: 10.1038/s41598-017-17156-w.

[27] S. Farhangfar, R. B. Yang, M. Pelletier, and K. Nielsch, "Atomic layer deposition of ZnS nanotubes," *Nanotechnology*, vol. 20, no. 32, 2009, doi: 10.1088/0957-4484/20/32/325602.

[28] M. Kumar and V. K. Lamba, "Structural and Elasticity Study of ZnS and ZnO Nanotubes Synthesized by Density Functional Method," no. July 2018, 2019.

[29] M. S. Khan, A. Srivastava, R. Chaurasiya, M. S. Khan, and P. Dua, “NH3 and PH3 adsorption through single walled ZnS nanotube: First principle insight,” *Chem. Phys. Lett.*, vol. 636, pp. 103–109, 2015, doi: 10.1016/j.cplett.2015.07.038.

[30] H. Zhang, S. Zhang, S. Pan, G. Li, and J. Hou, “A simple solution route to ZnS nanotubes and hollow nanospheres and their optical properties,” *Nanotechnology*, vol. 15, no. 8, pp. 945–948, 2004, doi: 10.1088/0957-4484/15/8/012.

[31] X. Zhang *et al.*, “Theoretical models of ZnS nanoclusters and nanotubes: First-principles calculations,” *Solid State Commun.*, vol. 147, no. 5–6, pp. 165–168, 2008, doi: 10.1016/j.ssc.2008.05.032.

[32] S. Park, G. J. Sun, H. Kheel, T. Ko, H. W. Kim, and C. Lee, “Light-activated NO2 gas sensing of the networked CuO-decorated ZnS nanowire gas sensor,” *Appl. Phys. A Mater. Sci. Process.*, vol. 122, no. 5, pp. 1–8, 2016, doi: 10.1007/s00339-016-0042-7.

[33] X. Zhang *et al.*, “First-principles study of ZnS nanostructures: Nanotubes, nanowires and nanosheets,” *Nanotechnology*, vol. 19, no. 30, 2008, doi: 10.1088/0957-4484/19/30/305708.

[34] Y. F. Zhu *et al.*, “Fabrication and photoelectrochemical properties of ZnS/Au/TiO2 nanotube array films,” *Phys. Chem. Chem. Phys.*, vol. 15, no. 11, pp. 4041–4048, 2013, doi: 10.1039/c3cp43572e.

[35] X. Chen *et al.*, “Wearable NO2 sensing and wireless application based on ZnS nanoparticles/nitrogen-doped reduced graphene oxide,” *Sensors Actuators, B Chem.*, vol. 345, no. 2, p. 130423, 2021, doi: 10.1016/j.snb.2021.130423.

[36] A. K. Giri, C. Charan, S. C. Ghosh, V. K. Shahi, and A. B. Panda, “Phase and composition selective superior cholesterol sensing performance of ZnO@ZnS nano-heterostructure and ZnS nanotubes,” *Sensors Actuators, B Chem.*, vol. 229, pp. 14–24, 2016, doi: 10.1016/j.snb.2016.01.060.

[37] E. C. Agwamba, K. Chukwuemeka, H. Louis, G. A. Okon, D. I. Eni, and A. L. E. Manicum, “Silicon Carbide and Its Germanium Dopant Nanocluster Derivatives as Sensors for Chloropicrin: Perception from Density Functional Theory and Monte-Carlo MD Simulation,” *Silicon*, vol. 16, no. 2, pp. 625–646, 2024, doi: 10.1007/s12633-023-02712-z.

[38] T. Zhai, Z. Gu, Y. Ma, W. Yang, L. Zhao, and J. Yao, “Synthesis of ordered ZnS nanotubes by MOCVD-template method,” *Mater. Chem. Phys.*, vol. 100, no. 2–3, pp. 281–284, 2006, doi: 10.1016/j.matchemphys.2005.12.044.

[39] S. Pal, B. Goswami, and P. Sarkar, “Electronic structure of ZnS nanotube: A density-functional study,” *Indian J. Phys.*, vol. 81, no. 10, pp. 1079–1093, 2007.

[40] N. Krainara, J. Limtrakul, F. Illas, and S. T. Bromley, “Structural and electronic bistability in ZnS single sheets and single-walled nanotubes,” *Phys. Rev. B - Condens. Matter Mater. Phys.*, vol. 83, no. 23, pp. 1–4, 2011, doi: 10.1103/PhysRevB.83.233305.

[41] H. Chen and C. Liu, “Stability, electronic and magnetic properties of ZnS nanotubes: a comparative study,” 2013.

[42] Q. An, X. Meng, K. Xiong, and Y. Qiu, “Self-powered ZnS Nanotubes/Ag Nanowires MSM UV Photodetector with High On/Off Ratio and Fast Response Speed,” *Sci. Rep.*, vol. 7, no. 1, pp. 1–12, 2017, doi: 10.1038/s41598-017-05176-5.

[43] T. Tsuneda, J. W. Song, S. Suzuki, and K. Hirao, “On Koopmans’ theorem in density functional theory,” *J. Chem. Phys.*, vol. 133, no. 17, 2010, doi: 10.1063/1.3491272.

[44] T. Banibairami, S. Jamehbozorgi, R. Ghiasi, and M. Rezvani, “Sensing Behavior of Hexagonal-Aluminum Nitride to Phosgene Molecule Based on Van der Waals–Density Functional Theory and Molecular Dynamic Simulation,” *Russ. J. Phys. Chem. A*, vol. 94, no. 3, pp. 581–589, 2020, doi: 10.1134/S0036024420030048.

[45] N. L. Hadipour, A. Ahmadi Peyghan, and H. Soleymanabadi, “Theoretical study on the Al-doped ZnO nanoclusters for CO chemical sensors,” *J. Phys. Chem. C*, vol. 119, no. 11, pp. 6398–6404, 2015, doi: 10.1021/jp513019z.

[46] Z. Rostami and H. Soleymanabadi, “Investigation of phosgene adsorption behavior on aluminum nitride nanocones: Density functional study,” *J. Mol. Liq.*, vol. 248, pp. 473–478, 2017, doi: 10.1016/j.molliq.2017.09.126.

[47] E. Vessally, R. Moladoust, S. M. Mousavi-Khoshdel, M. D. Esrafili, A. Hosseinian, and L. Edjlali, “Chloropicrin sensor based on the pristine BN nanocones: DFT studies,” *Struct. Chem.*, vol. 29, no. 2, pp. 585–592, 2018, doi: 10.1007/s11224-017-1055-3.

[48] A. Hosseinian, E. Vessally, M. Babazadeh, L. Edjlali, and M. Es’haghi, “Adsorption properties of chloropicrin on pristine and borazine-doped nanographenes: A theoretical study,” *J. Phys. Chem. Solids*, vol. 115, pp. 277–282, 2018, doi: 10.1016/j.jpcs.2017.12.036.

[49] V. Nagarajan and R. Chandiramouli, “Adamsite and chloropicrin molecular adsorption studies on novel green phosphorene nanotube – First-principles investigation,” *Chem. Phys.*, vol. 535, no. December 2019, p. 110782, 2020, doi: 10.1016/j.chemphys.2020.110782.

[50] A. Y. H. El, N. Ait, I. B. J. Mhalla, and A. El Habib, “Adsorption and reaction time effects on the properties of ZnS films grown by SILAR : an experimental study and DFT calculation,” *Opt. Quantum Electron.*, 2025, doi: 10.1007/s11082-024-07918-y.

[51] H. Xu, Z. Fan, Q. Liu, and L. Li, “Experimental study on photocatalytic CO2 reduction performance of ZnS/CdS-TiO2 nanotube array thin films,” *Open Chem.*, vol. 21, no. 1, 2023, doi: 10.1515/chem-2022-0306.

[52] F. I. Michos and M. M. Sigalas, “Computational study of the absorption spectrum of defected ZnS nanoparticles,” *J. Appl. Phys.*, vol. 123, no. 16, 2018, doi: 10.1063/1.5005589.

[53] M. A. S. Sakr, M. A. Saad, H. Abdelsalam, O. H. Abd-Elkader, L. Aleya, and Q. Zhang, “Two-Dimensional ZnS Quantum Dots for Gas Sensors: Electronic and Adsorption Properties,” *J. Electron. Mater.*, vol. 52, no. 8, pp. 5227–5238, 2023, doi: 10.1007/s11664-023-10455-1.

[54] S. Tarish *et al.*, “The shift of the optical absorption band edge of ZnO/ZnS core/shell nanotube arrays beyond quantum effects,” *J. Mater. Chem. C*, vol. 4, no. 7, pp. 1369–1374, 2016, doi: 10.1039/c5tc04152j.

[55] A. Es-Smairi, N. Fazouan, I. Bziz, and A. El Houssine, “DFT study of structural, electronic and optical properties of ZnS phases,” *Proc. 2018 6th Int. Renew. Sustain. Energy Conf. IRSEC 2018*, pp. 1–4, 2018, doi: 10.1109/IRSEC.2018.8702895.

[56] N. Dengo, A. Vittadini, M. M. Natile, and S. Gross, “In-Depth Study of ZnS Nanoparticle Surface Properties with a Combined Experimental and Theoretical Approach,” *J. Phys. Chem. C*, vol. 124, no. 14, pp. 7777–7789, 2020, doi: 10.1021/acs.jpcc.9b11323.